Published online 24 December 2012 Nucleic Acids Research, 2013, Vol. 41, No. 3 2047–2059
doi:10.1093/nar/gks1291

A small molecule directly inhibits the p53 transactivation domain from binding to replication protein A

Jason G. Glanzer[1], Katie A. Carnes[2], Patricia Soto[3], Shengqin Liu[1], Lawrence J. Parkhurst[2] and Gregory G. Oakley[1,*]

[1]Department of Oral Biology, College of Dentistry, University of Nebraska Medical Center, Lincoln, NE 68583, USA, [2]Department of Chemistry, University of Nebraska-Lincoln, Lincoln, NE 68588-0304, USA and [3]Department of Physics, Creighton University, Omaha, NE 68178, USA

Received July 30, 2012; Revised October 15, 2012; Accepted November 12, 2012

ABSTRACT

Replication protein A (RPA), essential for DNA replication, repair and DNA damage signalling, possesses six ssDNA-binding domains (DBDs), including DBD-F on the N-terminus of the largest subunit, RPA70. This domain functions as a binding site for p53 and other DNA damage and repair proteins that contain amphipathic alpha helical domains. Here, we demonstrate direct binding of both ssDNA and the transactivation domain 2 of p53 (p53TAD2) to DBD-F, as well as DBD-F-directed dsDNA strand separation by RPA, all of which are inhibited by fumaropimaric acid (FPA). FPA binds directly to RPA, resulting in a conformational shift as determined through quenching of intrinsic tryptophan fluorescence in full length RPA. Structural analogues of FPA provide insight on chemical properties that are required for inhibition. Finally, we confirm the inability of RPA possessing R41E and R43E mutations to bind to p53, destabilize dsDNA and quench tryptophan fluorescence by FPA, suggesting that protein binding, DNA modulation and inhibitor binding all occur within the same site on DBD-F. The disruption of p53–RPA interactions by FPA may disturb the regulatory functions of p53 and RPA, thereby inhibiting cellular pathways that control the cell cycle and maintain the integrity of the human genome.

INTRODUCTION

Genome stability requires the interplay of many signalling and DNA repair pathways, often requiring the action and regulation of multifunctional proteins that can modulate their activities appropriately during periods of DNA replication stress. Replication protein A (RPA), the major single-stranded DNA (ssDNA)-binding protein in eukaryotic cells, coordinates multiple DNA metabolic functions through interactions with numerous proteins critical to the DNA damage response (DDR) and DNA repair (1). RPA consists of three subunits (RPA70, RPA32 and RPA14) encompassing five ssDNA-binding domains (DBDs) that contribute to the high affinity of RPA binding to ssDNA (Figure 1) (2). RPA also has an affinity for dsDNA. *In vitro* experiments have shown that RPA binds to dsDNA and destabilizes the double helix, resulting in strand separation and RPA binding to ssDNA (3–5). The sixth identified binding domain, DBD-F, located on the N-terminus of RPA70, has been identified as the DBD primarily responsible for this destabilization activity of dsDNA (4). Although the precise mechanism of helix destabilization is not fully understood, the ability of DBD-F to bind ssDNA independently of the other DBDs with low affinity may be relevant to RPA unwinding activity (6). Additionally, DBD-F is a protein–protein interaction domain that is important in DNA repair and cell cycle checkpoint activities. A DBD-F mutant strain in yeast, *rfa-t11*, was found to be replication competent, but homologous recombination (HR) and checkpoint defective, suggesting that DBD-F was essential for specific DNA repair and the DDR signalling pathways, but not essential for replication in unstressed cells (7,8). Transient siRNA studies confirmed the importance of this domain in the DDR, as human cells expressing RPA70 with the analogous *rfa-t11* mutation resulted in replication comparable with cells expressing wt-RPA70; however, they were sensitive to camptothecin- and etoposide-induced replication stress (9,10).

*To whom correspondence should be addressed. Tel: +1 402 472 3519; Fax: +1 402 472 2551; Email: goakley@unmc.edu

The authors wish it to be known that, in their opinion, the first two authors should be regarded as joint First Authors.

© The Author(s) 2012. Published by Oxford University Press.
This is an Open Access article distributed under the terms of the Creative Commons Attribution License (http://creativecommons.org/licenses/by-nc/3.0/), which permits non-commercial reuse, distribution, and reproduction in any medium, provided the original work is properly cited. For commercial re-use, please contact journals.permissions@oup.com.

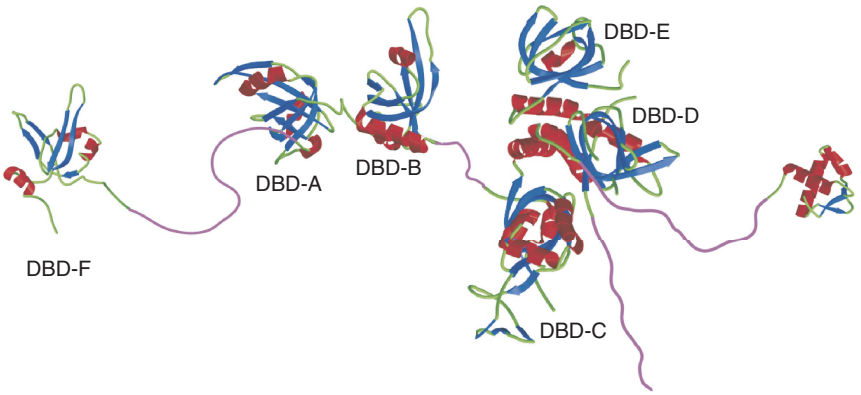

Figure 1. Illustration of the RPA heterotrimer depicting the oligonucleotide/oligosaccharide binding folds DBD-A through DBD-F. Modified from image provided by Dr Marc Wold.

The significance of DBD-F as a domain for protein–protein interactions was first described through an association with p53 (11–13). More recently, studies revealed that checkpoint activation, in part, is mediated through the recruitment of checkpoint proteins Rad9, ATR interacting protein (ATRIP) and Mre11 by DBD-F, as these proteins contain an amphipathic alpha helical domain that binds to the basic cleft of DBD-F (14–16). With the emergence of DBD-F as a recruiting scaffold for the assembly of DDR proteins, we have been interested in this domain as a novel target for cancer therapy, leading to our previous discovery of fumaropimaric acid (FPA) as an inhibitor of RPA protein interactions (17).

Tumour suppressor p53, the most commonly mutated gene in human cancers, primarily regulates the transcription of numerous genes involved in cell cycle control, apoptosis and DNA repair (18,19). p53 functions as a homotetramer and consists of DNA-binding and tetramerization domains that are flanked by two intrinsically disordered regions at both the N- and C-termini, the N-terminal transactivation and C-terminal regulatory domains, respectively (20). The N-terminal transactivation domain can be further divided into two subdomains, TAD1 (amino acids 1–40) and TAD2 (amino acids 41–61) (21). As TAD2 comes in contact with proteins containing DNA-binding domains, this intrinsically disordered region conforms to an amphipathic α-helix upon binding to proteins such as RPA (13,22). The p53TAD2 behaves as a ssDNA mimetic competing with ssDNA for binding to the DNA binding oligonucleotide/oligosaccharide-binding (OB) folds located within BRCA2 and RPA (23,24). Sequestration of p53 by BRCA2 and RPA has been suggested to inhibit the transcriptional activity of p53 with consequent down-regulation of apoptosis (25,26). Evidence for this model was demonstrated by overexpression of BRCA2 or a BRCA2 peptide that binds p53 and significantly reduced p53-mediated apoptosis (25). Conversely, the direct association of p53 with BRCA2 and RPA may interfere with HR independent of p53 transcriptional activity. This is supported by evidence that p53-mediated downregulation of replicative stress-dependent HR required p53 interaction with RPA (27).

Here, we show that DBD-F directly binds p53TAD2 and ssDNA, and that both of these interactions are inhibited by FPA. FPA binding results in a conformational shift in RPA occurring at a distant region from the binding surface. These results denote a more interactive relationship between DBD-F and other RPA domains than previously thought (28). We provide evidence that a double mutation (R41E and R43E) within DBD-F prevents both p53 binding and helix destabilization activity, suggesting that DBD-F may operate as a true protein-DNA binding domain *in vivo*. Molecular modelling simulations predict that DBD-F is highly flexible and is therefore susceptible to structural change due to ligand binding or subunit interactions. Finally, using a set of structurally related compounds, we have determined that both hydrophobic and electrostatic interactions play a role in the stability of the FPA–DBD-F complex formation.

MATERIALS AND METHODS

Reagents

5′ IRDye® 700 labelled polyT-30mer and unlabelled polyA-30mer oligonucleotides were purchased from Integrated DNA Technologies, Inc. The N-terminal X-rhodamine labelled p53TAD2, containing amino acids 40–57 (Xr-NH_2-MDDLMLSPDDIEQWFTED), was produced by AnaSpec. A p53TAD2 peptide containing an hemagglutinin (HA) tag (NH_2-MDDLMLSPDDIEQ WFTEDYPYDVPDYA) that does not contain an X-rhodamine label, referred to as p53TAD2-HA, was produced by Thermo Scientific. FPA and structurally related compounds were received from the Developmental Therapeutics Program of the National Cancer Institute.

Cloning, expression and purification of RPA, p53 and DBD-F fusion proteins

The human recombinant RPA and RPAΔF were purified from *Escherichia coli* as described previously (29). RPA containing the RPA70 mutations R41E and R43E, RPA (R41E, R43E), was generated using the Phusion®

site-directed mutagenesis kit (NEB), sequenced, and the corresponding protein purified accordingly. The maltose-binding protein (MBP) fusion protein containing amino acids 1–168 of DBD-F, referred to as DBD-F^{MBP}, was created by cutting out a NcoI/PstI RPA70 fragment from the RPA pET-11d vector, and ligating it into a pMBP-parallel2 expression vector (30). The resulting vector was expressed in *E. coli*, strain BL21, induced with isopropyl β-D-1-thiogalactopyranoside (IPTG), and purified using a gravity flow MBP-binding column (New England Biolabs). The concentrations of purified proteins were quantified using a Bradford assay. For expression of p53–GST fusion protein and unmodified GST, Addgene plasmid 10852 and pGEX-4T-1 were expressed in BL21 cells (31). After centrifugation, cells were sonicated in PBS in the presence of 1 mM PMSF and 1 mM DTT, clarified by centrifugation, and used directly in the binding assay. Characterization of the purified proteins, p53 and GST lysates, is shown in Supplementary Figure S4.

Electrophoretic mobility shift assays and helix destabilization assays

Electrophoretic mobility shift assays (EMSAs) for RPA, RPAΔF and RPA (R41E, R43E) were performed in binding buffer B (25 mM HEPES, 10% (v/v) glycerol, 10 mM NaCl, pH 8.0). The ssDNA probe is a 5′ IRDye® 700 labelled polyT-30mer oligonucleotide. To make the dsDNA probe, the labelled polyT-30mer was annealed to a polyA-30mer and treated with mung bean nuclease as reported previously (17). Concentrations of ssDNA and dsDNA probes were 20 nM. Concentrations of RPA were 10 nM and 40 nM for ssDNA and dsDNA binding, respectively. The concentrations of the RPA mutants were normalized relative to RPA ssDNA-binding activity. EMSAs for the DBD-F^{MBP} fusion protein were performed in binding buffer A (25 mM HEPES, 10% (v/v) glycerol, 100 mM NaCl, pH 8.0) with 2 μM DBD-F^{MBP} and electrophoresed at 4°C. Gels were scanned on a near infrared scanner, (LI-COR Biosciences).

Fluorescence anisotropy association curves

Data points were collected using a model A-1010 Alphascan photon counting fluorometer (Photon Technologies) in which the emission of the X-rhodamine-labelled p53TAD2 was monitored in binding buffer A at 25°C upon titration with RPA or DBD-F^{MBP}. The dye was excited using a xenon short arc lamp (Ushio, UXL-75XE, No. ME0282) followed by the excitation monochromator set at 585 nm (bandpass of ~5 nm). The exciting beam passed through a rotatable polarizer containing a mounted KN-36 Polaroid sheet (Polaroid) before reaching the sample cuvet. Emitted light was collected at 630 nm (bandpass of ~5 nm) after passing through a similar second polarizer (analyzer) placed between the sample cuvet and emission monochromator and photomultiplier (R928 PMT, Hamamatsu).

Each pair of intensity measurements, parallel (I_{VV}) and perpendicular (I_{VH}), was collected after the reaction reached equilibrium. The anisotropy values ($<r> = (I_{VV} - G \cdot I_{VH}) / (I_{VV} + 2 \cdot G \cdot I_{VH})$, where G is the grating factor (0.69 for X-rhodamine-labelled p53TAD2), reported are averages of three independent values at each point in the titration. For each intensity measurement, 30 data points were collected over a 1-s time period, fit by linear regression, and the fitted value at the midpoint, 0.5 s, was the recorded value for that time interval and used in determining the average over three such measurements. When there was no change in fluorescence, only anisotropy ($<r>$) was reported. Otherwise, the change in total fluorescence intensity (F, where $F = I_{VV} + 2 \cdot G \cdot I_{VH}$) or anisotropy multiplied by fluorescence intensity (rF, where $rF = <r> \cdot F$) was used to determine a binding constant (K_a) because these two functions are linear in concentrations of fluorescent species. The fraction (Y) of p53TAD2 bound to RPA or DBD-F^{MBP} was determined using the appropriate average signal ($<r>$, F or rF), and the best fit to a single binding site model (Equation 1) was obtained by a least squares minimization where K_a and $<r>_{max}$ are parameters. For instance,

$$\begin{aligned} Y_{(i)} &= (<r>_{obs(i)} - <r>_{min})/(<r>_{max} - <r>_{min}) \\ &= [(R_{T(i)} - Y_{(i)} \cdot P_{T(i)}) \cdot K_a]/[1 + K_a \cdot (R_{T(i)} - Y_{(i)} \cdot P_{T(i)})] \end{aligned} \quad (1)$$

where $<r>_{obs(i)}$ is the average anisotropy at iteration i, $<r>_{min}$ and $<r>_{max}$ are the minimum and maximum anisotropies, R_T is the total concentration of protein (RPA or DBD-F^{MBP}) and P_T is the total concentration of p53TAD2. Equation 1 can be rearranged into a quadratic form (Equation 2):

$$\begin{aligned} 0 = &-Y_{(i)}^2 \cdot K_a \cdot P_{T(i)} + Y_{(i)} + Y_{(i)} \cdot K_a \cdot P_{T(i)} \\ &+ Y_{(i)} \cdot K_a \cdot R_{T(i)} - R_{T(i)} \cdot K_a, \end{aligned} \quad (2)$$

where the quadratic coefficients are: $a = -K_a \cdot P_T$, $b = (1 + P_T \cdot K_a + R_T \cdot K_a)$, $c = -R_T \cdot K_a$ and Y can then be solved using the familiar quadratic equation with the positive sign proceeding the radical. K_d is the concentration of free ligand at which Y = 0.5 and $K_d = 1/K_a$. When the binding is weak and the concentration of fluorescent ligand is low, Equation 1 can be simplified as shown in Equation 3, also with two parameters, K_a and $<r>_{max}$:

$$\begin{aligned} Y_{(i)} &= (<r>_{obs(i)} - <r>_{min})/(<r>_{max} - <r>_{min}) \\ &\approx [R_{T(i)} \cdot K_a]/[1 + K_a \cdot R_{T(i)}] \end{aligned} \quad (3)$$

Parameter errors reported are one standard deviation. For data sets with fewer than 20 points, the confidence region was obtained by applying the Student's t-test. The concentrations were adjusted for any dilution effects.

Tryptophan fluorescence quenching

Quenching of tryptophan fluorescence was used to determine direct binding of FPA to RPA and aid in determining whether both ligands could simultaneously be bound to RPA. The fluorescence of the sample, 3 μM RPA upon addition of FPA in binding buffer A at 25°C, was collected using the same apparatus as for the fluorescence anisotropy data, with an excitation wavelength of

292 nm. For the emission wavelengths, a single value at every 1 nm was collected from 325–375 nm and data were smoothed using a Savitzky–Golay quadratic smoothing function with a 7-point filter. The average of 5–8 smoothed buffer fluorescence intensity values at 348 nm was subtracted from the average of 5–8 similarly smoothed sample values and the difference for each data point recorded ($F_{obs(i)}$). The data points were fit according to the single binding site model (Equation 3) with two parameters (F_{min} and K_a), where $Y_{(i)} = 1 - [(F_{obs(i)} - F_{min}) / (F_{max} - F_{min})]$, $F_{obs(i)}$ is the total observed fluorescence at iteration i, F_{min} and F_{max} are the minimum and maximum fluorescence respectively and $Y_{(i)}$ is the fraction of RPA bound to FPA. The reported K_d is calculated from K_a ($K_d = 1/K_a$). The concentrations were adjusted for any dilution effects.

Fluorescence anisotropy competition curves

Data points were collected with the same apparatus and method as described for the association curves where X-rhodamine-labelled p53TAD2 is the reporter. Samples were incubated after each addition of the competing ligand at 25°C until equilibrium was reached.

The data set was fit assuming the simplest model: binding of p53TAD2 and FPA to the DBD-F^{MBP} in the full-length RPA is competitive and exclusive. A Newton–Raphson matrix routine (32) for two nonlinear binding equations and the associated Jacobian (J) embedded in a two-dimensional least squares grid search was used to determine two optimal and correlated K_a's and the joint 68% confidence region for the competition experiment involving RPA, p53TAD2 and FPA. Subsequently the same procedure was followed for the DBD-F^{MBP} using both FPA and p53TAD2-HA as the competing ligands. The Newton–Raphson was constrained by the conservation of the total concentrations of the three species (Equations 4–6):

$$R_{T(i)} = R_{(i)} \cdot (1+K_{a1} \cdot P_{(i)}+K_{a2} \cdot FPA_{(i)}); \; R_{(i)} = R_{T(i)}/L \quad (4)$$

$$P_{T(i)} = P_{(i)}+K_{a1} \cdot P_{(i)} \cdot R_{(i)} = P_{(i)} \cdot G_{1(i)}, \quad \text{where } G_1 = 1+(K_{a1} \cdot R_{T(i)})/L \quad (5)$$

$$FPA_{T(i)} = FPA_{(i)}+K_{a2} \cdot FPA_{(i)} \cdot R_{(i)} = FPA_{(i)} \cdot G_{2(i)}, \quad \text{where } G_2 = 1+(K_{a2} \cdot R_{T(i)})/L \quad (6)$$

where R_T, P_T and FPA_T are the total concentrations and R, P and FPA are the free concentrations of RPA, p53TAD2 and FPA, respectively, for each iteration (i), L is the binding polynomial based on the simplest model ($1+K_{a1} \cdot P_{(i)}+K_{a2} \cdot FPA_{(i)}$), and $K_{a1}$and K_{a2} are the binding constants of p53TAD2 binding to RPA and FPA binding to RPA, respectively.

The above three conservation conditions reduce to two equations (Equations 5 and 6) that generate the two Newton–Raphson equations (Equations 7 and 8). F_1 and F_2, the concentrations of free p53TAD2 and FPA respectively, equal zero when the concentrations are correctly determined in the Newton–Raphson routine. For instance,

$$F_{1(i)} = P_{T(i)} - P_{(i)} \cdot G_{1(i)} \quad (7)$$

$$F_{2(i)} = I_{T(i)} - FPA_{(i)} \cdot G_{2(i)} \quad (8)$$

The Jacobian matrix ($J_{i,j} = \partial F_i/\partial X_j$, $X_1 = (P)$, $X_2 = (FPA)$) is defined by $J_{1,1} = a$, $J_{1,2} = b$, $J_{2,1} = c$ and $J_{2,2} = d$. The four quantities are identified as: $a = -G_1 + P_{(i)} \cdot (K_{a1}{}^2 \cdot R_{T(i)}) / L^2$, $b = P_{(i)} \cdot K_{a1} \cdot R_{T(i)} \cdot K_{a2} / L^2$, $c = FPA_{(i)} \cdot K_{a2} \cdot R_{T(i)} \cdot K_{a1} / L^2$, $d = -G_2 + FPA_{(i)} \cdot K_{a2}{}^2 \cdot R_{T(i)} / L^2$. The inverse Jacobian matrix (J^{-1}) is then: $J^{-1}{}_{1,1} = d / \Delta$, $J^{-1}{}_{1,2} = -b / \Delta$, $J^{-1}{}_{2,1} = -c / \Delta$ and $J^{-1}{}_{2,2} = a / \Delta$, where delta is the determinant of J ($\Delta = a \cdot d - b \cdot c$).

The Newton–Raphson algorithm (Equation 9) uses known values of $P_{T(i)}$, $FPA_{T(i)}$ and $R_{T(i)}$ and chosen values of K_{a1} and K_{a2} where iterations (i) proceed to convergence where $F_1 = F_2 = 0$.

$$V_{(i+1)} = V_{(i)} - J^{-1} \cdot F_{(i)} \quad (9)$$

where V is a column vector with rows P and FPA, and F is a column vector with rows F1 and F2.

The optimal K_{a1} and K_{a2} values were used to calculate the fraction of p53TAD2 bound to RPA and then converted to a response function (Equation 10) in order to determine the sum of squared residuals with respect to $<r>_{obs}$:

$$<r>_{calc(i)} = <r>_{min} \cdot P_{(i)}/P_{T(i)} + <r>_{max} \cdot (P_{T(i)} - P_{(i)})/P_{T(i)} \quad (10)$$

The maximum or minimum signal in the absence of the competing ligand was determined before titration. Excellent endpoints were obtained using a conventional double-reciprocal plot and refined using a one-dimensional grid search added to the Newton–Raphson routine. The square root of the minimum sum of the squared residuals (σ_{best}) was thus determined. Subsequent grid searches were carried out varying the binding constants until Equation 11 (33) was satisfied for the 68% confidence boundary ($\sigma_{68\%}$):

$$\sigma_{68\,\%} = \sigma_{best} \cdot (1+(p/(n-p)) \cdot F_{p,n-p,0.32})^{0.5} \quad (11)$$

with n data points, p parameters, and the critical F value was calculated using an online F distribution calculator (http://www.danielsoper.com/statcalc3/calc.aspx?id=4) with p degrees of freedom in the numerator and (n−p) degrees of freedom in the denominator. Significant overlap between the 68% confidence regions of the individually determined K_d values and the K_d values from the competition experiment validates the assumption of the competitive and exclusive binding model. Therefore, the same program was used to analyse the competitive binding data involving the DBD-F^{MBP}. As the DBD-F^{MBP} does not have a tryptophan, direct binding of FPA cannot be determined using tryptophan fluorescence quenching, and a competition experiment must be used to determine the K_d for the binding of FPA to the DBD-F^{MBP}. The 68% ellipsoidal confidence region for the

K_d values of p53TAD2/ DBD-F^{MBP} and FPA/ DBD-F^{MBP} was truncated by the 68% confidence region of the individually determined p53TAD2 and DBD-F^{MBP} K_d, leaving part of an ellipsoid as our final 68% confidence region. The same analysis was used to determine the K_d and 95% confidence region ($\sigma_{95\%} = \sigma_{best} * (1 + (p/(n-p)) * F_{p,\, n-p,\, 0.05})^{0.5}$) for the competitive binding between X-rhodamine-labelled p53TAD2 and p53TAD2-HA.

Protein modelling and docking

The protein structure (PDB ID: 2B29), composed of residues 1–121 of RPA70, was relaxed using all-atom molecular dynamics (MD) simulations. All MD simulations were performed using the GROMACS 4.5.1 package (34). The AMBER96 force field (35) was used to describe the protein structure and the tip3p water model to describe the solvent (36). Protein charge states were set in accordance with a pH of 7, and no counter ions were added (37). The protein was solvated in a periodic dodecahedron-shaped box with ~5300 water molecules and energy minimized for 200 steps using the steepest descent algorithm. A 0.1-ns-long position restrained MD simulation was followed by a 1-ns-long MD simulation in the moles (N), volume (V) and temperature (T) (NVT) ensemble. The temperature was maintained close to 300 K by weak coupling to an external temperature bath (38) with a coupling constant of 0.1 ps. The LINCS (39) algorithm was used to constrain bond lengths within the solute. The SETTLE (40) algorithm was used to constrain the bond lengths and the bond angle in water. The integration time step was 2 fs. The reaction field method (41) [reaction-field-zero as implemented in GROMACS 4.5.1 (42)] was used to account for electrostatic interactions with a twin-range cut-off of 0.9/1.2 nm. Interactions within the short-range cut-off were evaluated at every step, whereas interactions within the long cut-off were updated every five steps, together with the pair list. The equations of motion were integrated using the leapfrog algorithm. The snapshot at 1.0 ns from the NVT simulation was used as input for the anisotropic normal mode analysis (ANM) (43) calculation. The all-atom ANM calculation was implemented using the ProDy package (44), with a cut-off value of 15 Å and a uniform force constant. The non-trivial three slowest modes were used to generate a 200-conformer ensemble within a root-mean-square value of 3.0 Å. Subsequently, each conformer was energy minimized in the gas phase for 200 steps. The top 100 structures that displayed proper stereochemistry were used in a docking simulation with the structure for FPA using the virtual screening software, PyRx, in conjunction with the docking software, AutoDock Vina (45,46). Affinity scores in PyRx are reported as binding energies (ΔG), which were then converted to apparent inhibitory constants (K_i) through the equation, $K_i = e^{(\Delta G/RT)}$, where T = 298.15 K and R = 0.001968 kcal/mol/K. The top scoring DBD-F structure was compared with the original 2B29 structure in docking both FPA and a portion of the p53TAD, $_{40}$MDDLMLSPDDI$_{51}$, and graphically reported using the software program Pymol (47).

Full length p53 binding assays

Clarified bacterial lysate (100 µl) expressing GST or p53–GST was added to each well of a glutathione-coated 96 well plate (Pierce). After 30 min, the plate was washed 3× with PBST (PBS, 0.1% tween-20), then incubated for 30 min in PBS with 250 nM RPA. Plates were washed 3× with PBST and incubated with a polyclonal antibody for GST (kindly provided by Dr James Wahl, 1:100), and RPA70 (Bethyl, 1:1000) for 30 min. Wells were washed 3× with PBS and incubated with secondary fluorescent antibodies Alexa Fluor 680 (Invitrogen, 1:1000) and Dylight 800 (ThermoScientific, 1:1000). Wells were washed 3× with PBST and scanned on near infrared scanner (LI-COR Biosciences). Binding efficiency was determined by the amount of RPA signal normalized to GST signal. Western blots of bacterial lysates are shown in Supplementary Figure S4.

RESULTS

FPA, p53 and ssDNA compete for binding to RPA

We previously demonstrated that FPA prevented helix destabilization by RPA (17). A potential explanation for the loss of helix destabilization by RPA is that FPA binds to DBD-F and prevents DBD-F–ssDNA intermediates from forming before ssDNA binding by the high affinity DBDs. To test this model, we separated RPA into two ssDNA-binding entities, a heterotrimer without DBD-F (RPAΔF) and DBD-F fused to MBP (DBD-F^{MBP}). The capacity of FPA to selectively inhibit ssDNA binding to DBD-F^{MBP} and not RPAΔF was observed via EMSA (Figure 2A and B). MBP alone does not bind ssDNA (Supplementary Figure S1A). Combined, these data indicate that the mechanism of DNA unwinding by RPA is dependent on DBD-F, and suggest that a peptide that mimics ssDNA, such as p53TAD2, should also be an effective inhibitor of helix destabilization. Indeed, an X-rhodamine-labelled p53TAD2 peptide inhibited helix destabilization (Figure 2C). p53TAD2 was not effective in preventing the binding of RPA to ssDNA, indicating p53TAD2 does not compete with ssDNA for binding to the central high affinity DNA binding core, DBD-A and B (Figure 2D). The band observed directly above the free dsDNA probe was determined to be due to the fluorescence of the X-rhodamine label of the p53TAD2 peptide and does not interact with dsDNA or have helix destabilization activity (Supplementary Figure S1B). These data suggest that protein–protein interactions at the DBD-F would have an effect on some aspect of DNA processing by RPA, and that FPA can inhibit both types of substrates, proteins and ssDNA, from interacting with the DBD-F.

Effect of FPA analogues on RPA and DBD-F^{MBP} binding

With the evidence of FPA directly binding and inhibiting the DBD-F, we attempted to determine the structural components of this compound that are essential for activity. A survey of the Open Chemical Repository of the Developmental Therapeutics Program at the

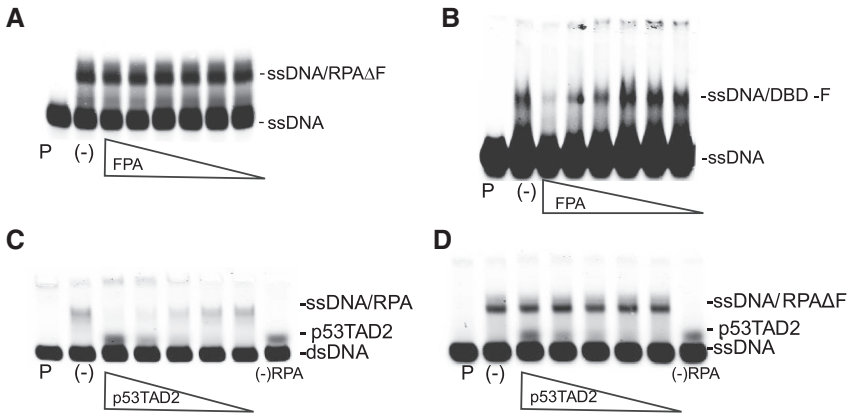

Figure 2. p53TAD2 and FPA bind to DBD-F^{MBP} and RPA and affect DNA binding. For (A–D): Lane with DNA probe in the absence of RPA is denoted by 'P'. ssDNA–RPA binding without FPA is marked by a (-). Concentration of labelled DNA probe is 10 nM. For (A) and (B), the concentration of FPA is 300, 100, 30, 10, 3, 1 μM, respectively. (**A**) Lack of inhibition of ssDNA–RPAΔF formation in the presence of FPA as determined by EMSA. The concentration of RPAΔF is 20 nM. (**B**) Inhibition of ssDNA–DBD-F^{MBP} binding by FPA. The concentration of the DBD-F^{MBP} is 2 μM. For (C) and (D), the p53TAD2 concentration is 24, 12, 6, 3, 1.5 μM, respectively. (**C**) Inhibition of helix destabilization by p53TAD2. The amount of helix destabilization was determined by the appearance of an upward shifted band consisting of RPA bound to unwound ssDNA derived from dsDNA. Lane with labelled DNA and p53TAD2 in the absence of RPA is denoted by a '*'. (**D**) Lack of inhibition of ssDNA–RPA binding by p53TAD2. The p53TAD2 peptide can be detected at higher concentrations due to the fluorescence of the x-rhodamine label, and does not bind DNA, as determined in figure S3C.

National Cancer Institute (NCI) identified seven structural analogues of FPA, referred to in the NCI databank as NSC15520 (Figure 3A). All of the compounds have at least three fused six-membered rings, and three compounds have nearly exact structural backbones as that of FPA, but have substituted the 1,4-dicarboxylic acid with an anhydride (NSC204220), a 1,4-diol (NSC49890), or a 1,4-dione (NSC2961) (Figure 3A, #s 2, 4 and 5). The anhydride-containing NSC98616 has a slightly altered backbone structure as well as a hydroxyl group substituted for the singular carboxyl group (Figure 3A, # 3). Also included in the study were three abietic acid analogues (NSC4827, NSC5007, NSC18746) (Figure 3A, #s 6, 7 and 8), as abietic acid provides the backbone structure in the reaction with fumaric acid to create FPA (48).

When assayed for helix destabilization activity, four compounds (FPA, the diol-containing NSC49890, and the anhydride compounds NSC204220 and NSC98616) inhibited helix destabilization by RPA (Figure 3B, top panel, lanes 1–4), but only FPA showed no evidence of inhibiting RPA binding to ssDNA (Figure 3B, bottom panel, lane 1). These data indicate that only FPA, with the 1,4-dicarboxylic moiety, is capable of selectively inhibiting DBD-F of RPA, whereas the other compounds (NSC204220, NSC98616, NSC49890) likely bind to residues within the other DBDs, A–E. Abietic acid analogues NSC4827, NSC5007 and NSC18746 showed no effect on RPA helix destabilization and ssDNA binding, suggesting that either the transition of abietic acid to a nonplanar molecule, the addition of negatively charged moieties, or both, are required for RPA inhibition. NSC2961, a 1,4-dione, also did not interact with RPA, accentuating the importance of the 1,4-dicarboxylic acid for inhibition of DBD-F.

The binding of FPA and structural analogues of FPA to DBD-F^{MBP} was also investigated through fluorescent anisotropy. Here, compounds were tested for the ability to inhibit binding of p53TAD2 to DBD-F^{MBP}. Of the compounds tested, FPA showed the most potent inhibition compared with the other seven compounds, further supporting FPA as a DBD-F-specific inhibitor (Table 1).

Because the 1,4-dicarboxylic acid moiety appears to be essential for the binding activity of FPA with DBD-F^{MBP}, we compared the specificity of FPA with other 1,4-dicarboxylic acids (Figure 3C). In these experiments, both 1,4-cyclohexanedicarboxylic and succinic acids (Figure 3C, compounds 1 and 2, respectively) are FPA sub-structures. These three compounds were analysed for their ability to inhibit the helix destabilization activity of RPA (Figure 3D). As anticipated, FPA inhibited helix destabilization of a dsDNA template by RPA, whereas 1,4-cyclohexanedicarboxylic and succinic acids had no effect (Figure 3D, lane 3). To further confirm the selective inhibition of FPA, we performed competitive titration assays using fluorescence anisotropy. Only FPA competed with X-rhodamine-labelled p53TAD2 for binding to DBD-F^{MBP}, as reported in Table 1, with 1,4-cyclohexanedicarboxylic and succinic acids showing no evidence of binding (data not shown). Taken together, these results show that both the electrostatic charge of the dicarboxylic acid moiety and the hydrophobic backbone of FPA are necessary for binding to DBD-F^{MBP}.

FPA and p53TAD2 directly bind to RPA independently and competitively

The ability of FPA to inhibit DBD-F binding to ssDNA suggested, but did not prove, a direct interaction of FPA with full length RPA. To assess direct binding to full length RPA, we determined the ability of FPA to quench tryptophan residues within RPA (Table 2, Supplementary Figure S2C). The addition of FPA to

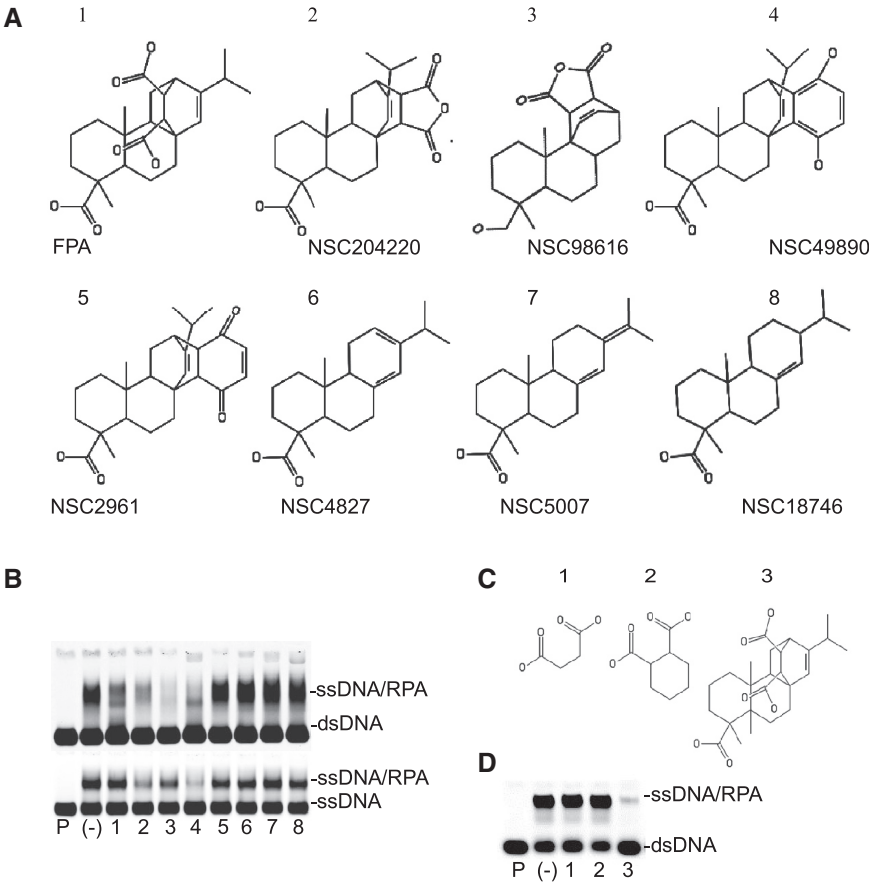

Figure 3. Effect of structural analogues of FPA on DBD-F^{MBP} inhibition. (**A**) Structures of lead compound FPA and structural analogues used in this study. (**B**) Effect of FPA-related compounds on DNA binding as measured by EMSAs. 200 μM of each compound was used. Top panel: addition of dsDNA to compounds preincubated with RPA. Bottom panel: addition of ssDNA to compounds preincubated with RPA. Lane with DNA in the absence of RPA is demarked by 'P'. RPA–DNA binding without inhibitor is marked by a (-). Numbers correspond to structures in 'A'. (**C**) Structure of FPA sub-structures succinic acid, 1,4-cyclohexanedicarboxylic acid and FPA (1–3, respectively). (**D**) Effect of compounds in 'C' (200 μM) on helix destabilization via EMSA. Lane with ssDNA probe in the absence of RPA is demarked by 'P'. RPA–DNA binding without inhibitor is denoted by a (-).

Table 1. K_d values for FPA and derivatives binding to DBD-F^{MBP} prebound to p53TAD2 as determined by fluorescence anisotropy

#	Inhibitor	K_d (μM)	SD (μM)
1	FPA	9.0	1.2
2	NSC204220	103	9
3	NSC98616	ND	ND
4	NSC49890	ND	ND
5	NSC2961	ND	ND
6	NSC4827	ND	ND
7	NSC5007	ND	ND
8	NSC18746	660	250

ND, not determined.

RPA resulted in the quenching of the fluorescence of one or more tryptophan residues within RPA, allowing the binding constant of FPA to RPA to be determined ($K_d = 29.0 \pm 3.5$μM). DBD-F itself does not contain tryptophan residues. Therefore, these data do not confirm direct binding to DBD-F itself; however, based on our previous data (17) and the other data presented here, it suggests that the quenching of tryptophan by FPA in RPA is likely due to a conformational change induced by direct binding, and not by a direct interaction of tryptophan with the inhibitor.

To assert that p53TAD2 and FPA compete for the same binding site, we conducted fluorescence anisotropy titrations. We observed X-rhodamine-labelled p53TAD2 bound to RPA (Supplementary Figure S2A). In a competition assay, addition of FPA to a preformed p53TAD2–RPA complex resulted in a decrease in anisotropy, indicating that FPA bound to RPA, replacing p53TAD2 (Supplementary Figure S2B). A Newton–Raphson matrix routine for two nonlinear binding equations was embedded in a two-dimensional least squares grid search in order to determine the two optimal binding constants and determine the joint 68% confidence region for FPA ($K_d = 29.0 \pm 3.5$ μM) and p53TAD2 ($K_d = 6.06 \pm 0.08$ μM). Increasing concentrations of FPA up to 275 μM showed no evidence of binding to p53TAD2 (Supplementary Figure S3A). The competition experiment showed no evidence for joint occupancy of p53TAD2 and FPA in the DBD-F of the full length RPA, and was determined to be a valid method for determining the affinity of a ligand by replacement of a competing fluorescent ligand. These results demonstrate

that FPA binds directly to RPA, and that both FPA and p53TAD2 bind RPA independently and competitively.

p53TAD2 and FPA bind specifically to the DBD-F of RPA

To ensure that the competition between FPA and p53TAD2 for RPA is specific for DBD-F, their respective binding to DBD-F^{MBP} was explored. The p53TAD2 bound to DBD-F^{MBP} with high affinity (K_d of 1.03 ± 0.25μM) as determined by fluorescence quenching of the X-rhodamine label (Table 2 and Supplementary Figure S2D, filled circles). Addition of MBP to p53TAD2 gave no change in fluorescence under similar concentrations (Supplementary Figure S2D, hollow circles). These results showed that the isolated DBD-F^{MBP} is competently folded for binding protein.

FPA binding to DBD-F could not be detected directly, as there were no tryptophans in DBD-F. Therefore, a fluorescence anisotropy competition assay was used to determine the affinity of FPA for DBD-F^{MBP}. The fraction of p53TAD2-bound DBD-F^{MBP} decreased upon addition of FPA (Supplementary Figure S2E). From these findings, the two binding constants for both ligands were determined to be K_d values at 1.2 and 9.0 μM, respectively (Table 2 and Supplementary Figure S2F).

In comparison with full length RPA, DBD-F^{MBP} had substantially higher affinity for both p53TAD2 and FPA than the full length RPA (6-fold and 3-fold, respectively). A similar competition experiment involving X-rhodamine-labelled p53TAD2 and p53TAD2-HA showed that the K_d values for binding DBD-F^{MBP} were not significantly different at the 95% confidence level. Therefore, the presence of the X-rhodamine dye on the N-terminus of p53TAD2 did not significantly alter binding (K_d = 0.67 μM, data not shown). Furthermore, the critical amino acids for contacting the DBD-F are indeed within the p53TAD2, as addition of the 10 amino acids of the HA tag did not alter binding.

R41E and R43E mutations in RPA70 reveal the specific nature of DBD-F for protein, DNA and FPA

Evidence for the requirement of DBD-F in recombination was first derived from the yeast strain rfa-t11, containing a K45E mutation in Rfa1, the yeast homolog of RPA70 (49). Although it has been inferred that the mutation causes the interruption of RPA with several RPA substrates such as p53, only Ddc2, the yeast homolog of ATRIP, has been shown to be directly affected by the mutation using full length proteins (50), and protein–protein interaction studies involving full length human RPA with analogous mutations to rfa-t11 have not been demonstrated. To confirm that FPA interactions with human RPA are specific to the analogous K45 mutation of rfa-t11, we generated a glutamic acid-substituted mutant (R41E, R43E), as NMR studies have indicated that both residues are essential for p53TAD2 binding (51).

The double mutant retained the ability to bind ssDNA, as no amino acid substitutions were made on the high-affinity DBDs (Figure 4A, left panel). When tested for helix destabilization activity, the mutant was limited in unwinding DNA, similar to RPAΔF (Figure 4A, right panel). The small amount of unwinding observed was not further inhibited by FPA at concentrations up to 1 mM, suggesting that the nominal unwinding that does occur by RPA (R41E, R43E) is DBD-F independent. The R41E and R43E mutations highlight their importance in helix destabilization, and strongly suggest that the recombination deficient rfa-t11 yeast strain likewise contains an RPA that is deficient in this activity.

To determine whether the RPA (R41E, R43E) mutation has an effect on p53 binding, we devised an ELISA-based binding assay (Figure 4C and D). Wild-type RPA bound readily to the immobilized p53–GST fusion protein, and was effectively inhibited from binding to p53 by FPA at 100 μM. GST alone does not bind RPA (Supplementary Figure S3B). In a comparison of RPA, RPAΔF and RPA (R41E, R43E), only RPA was capable of effectively binding p53–GST. These data support R41 and R43 as essential residues in DBD-F for p53 binding.

We then tested whether RPA (R41E, R43E) would undergo tryptophan quenching in the presence of FPA (Table 2 and Figure 4E). Half-maximal quenching was seen at a concentration of 230 μM, approximately 8-fold higher concentration than required for RPA. This suggests that the double mutation affects the ability of RPA to change conformation in the presence of FPA, providing further evidence of FPA specificity for DBD-F.

Table 2. K_d values of DBD-F^{MBP} and various RPAs for RPA and p53TAD2 substrates as determined by either fluorescence quenching or fluorescence anisotropy

Protein	Substrate	K_d (μM)	SD (μM)	Method[a]
RPA	FPA	29.0	3.5	1
RPA	p53TAD2	6.06	0.08	2
DBD-F	p53TAD2	1.03	0.25	1
DBD-F	FPA	9.0	1.2	2
RPAΔF	FPA	>400	NA	1
RPA(R41E,R43E)	FPA	230	18	1
DBD-F[b]	p53TAD2	99.9	8.4	2
DBD-F[b]	FPA	18.3	0.9	2

[a](1)Fluorescence quenching; (2)Fluorescence anisotropy.
[b]From Souza-Fagundes *et al.* (63).

Modelling of the DBD-F reveals large scale changes within the basic cleft

The ability of DBD-F to bind several disparate ligands (ssDNA, FPA, proteins) suggests that the domain possesses structural and dynamic features. Recent work suggests that conformational changes at the binding site are often responsible for the ability of proteins to bind different ligands (52,53). Using MD simulations, we determined the extent by which DBD-F is susceptible to conformational change (Figure 5). The original crystal structure of DBD-F shows a wide gap within the basic cleft, with the walls of the cleft opening outward, creating a large area for binding (24) as represented in Figure 5A. However, when analysed by docking software, FPA was predicted to bind with low affinity (K_i = 204.7 μM) at a position adjacent to the cleft.

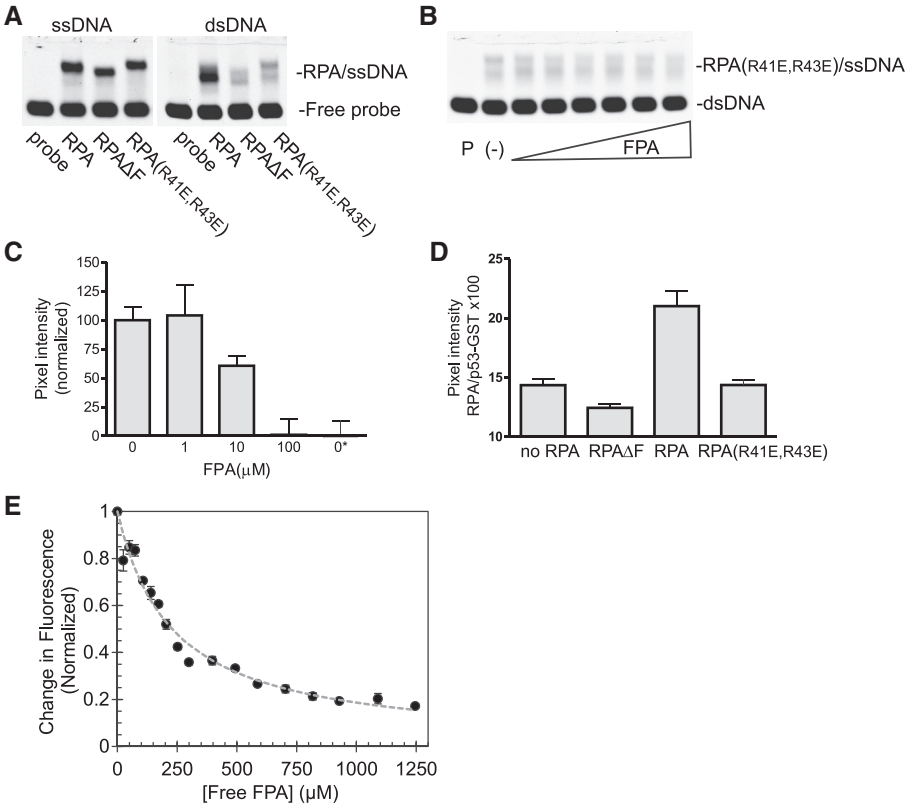

Figure 4. The K41E,K43E mutation affects RPA binding to protein, DNA and FPA. (**A**) Left panel: wild-type RPA and two mutant RPAs are all capable of competently binding ssDNA via EMSA. Right panel: only wild-type RPA is capable of effectively unwinding dsDNA. (**B**) The small amount of dsDNA that is unwound by RPA (R41E, R43E) is not effected by moderate concentrations of FPA. Concentrations of FPA are 31, 62, 125, 250, 500, 1000 μM, respectively. (**C**) ELISA-based assay showing the ability of FPA to prevent p53 binding to full length RPA. Bacterial lysates expressing p53–GST were bound to a glutathione-coated plate, and then incubated with 250 nM RPA in the presence of the indicated concentration of FPA. 100% RPA signal is normalized to wells with 0 μM inhibitor. 0% RPA signal is normalized to the absence of RPA (0*). Error bars represent the standard error of the mean. (**D**) RPA(R41E, R43E) and RPAΔF are unable to bind p53 as determined by assay described in 'A'. (**E**) Tryptophan quenching of RPA(K41E,K43E) by FPA. K_d = 230 μM ± 18 μM.

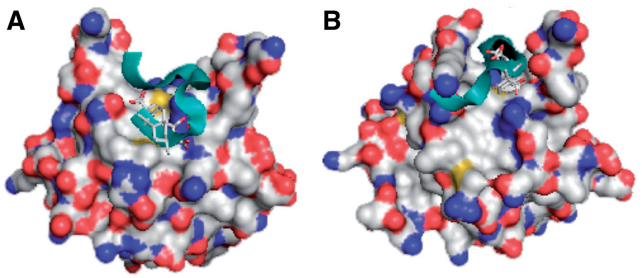

Figure 5. Docking simulations of a crystal structure of DBD-F and conformer optimized for FPA binding. For both structures, FPA is shown in stick form, whereas the p53TAD2 sequence 'MDDLMLSPDDI' is represented by a ribbon structure. (**A**) The original crystal structure of DBD-F docked to FPA and p53TAD2 [−5.5 and −4.4 kcal/mol (24.5 μM and 204.7 μM), respectively]. (**B**) A DBD-F model optimized for FPA binding docked FPA and p53TAD2 [−6.6 and −5.9 kcal/mol (2.9 μM and 11.3 μM), respectively].

A portion of the p53TAD2 predictively bound at higher affinity (K_i = 24.5 μM), but does not lie in line with the basic cleft of DBD-F (Figure 5A).

When MD simulations were used to find alternative conformations of the DBD-F, a DBD-F representation predicted to bind FPA at 18-fold greater affinity was found (K_i = 11.3 μM) (Figure 5B). This representation possessed a basic cleft in a more restricted conformation, with the walls of the cleft almost wrapping around the inhibitor. The p53TAD2 peptide also was predicted to bind at 8-fold higher affinity (K_i = 2.9 μM) than to the original crystal structure of DBD-F, enveloping the predicted binding site of FPA. Though the docking scores should be considered as a relative ranking parameter, they do suggest that the newly ascribed DBD-F representation may be more accurate than the original crystal structure. This new representation of DBD-F may help to explain the exclusive binding of dissimilar ligands and provide a more accurate model for DBD-F *in vivo*.

DISCUSSION

The ability of multiple ligands to bind DBD-F is an example of DNA and protein mimicry common to DNA repair pathways, allowing RPA to 'hand-off' multiple DNA and protein substrates (54). RPA–p53 interactions are required for maintaining a balance between pathways that repair double strand breaks, as mutations in the p53TAD2 that prevent RPA binding result in

excessive homologous recombination (55). This hyper-recombination phenotype can lead to genomic instability and cell death (56,57). An inhibitor to the DBD-F may have a similar destabilizing effect on cancer cells to that of the p53TAD2 mutant. As other proteins involved in homologous recombination also bind the DBD-F such as Mre11 and Nbs1 (10,14), it is likely that a DBD-F inhibitor, such as FPA, could have the ability to deregulate homologous recombination, allowing the selection of normal cells that have competent and redundant DNA repair pathways over cancer cells that typically have reduced DNA repair capacity.

Two components of FPA appear to be essential for the inhibition of DBD-F. The dicarboxylic moiety of FPA likely interacts with the positively charged residues of the DBD-F, R41 and R43, as removal or alteration of the moiety to hydroxyl, aldehyde or anhydride eliminates either the action or specificity of the compound to DBD-F. The backbone of FPA, derived from abietic acid, provides a complex hydrophobic helical structure that likely fits within the hydrophobic residues of DBD-F. The negatively charged and hydrophobic components of FPA combine to resemble both the ssDNA and peptide substrates of DBD-F. Further studies will entail modifications in both charged and uncharged components of FPA in newly synthesized compounds that allow for higher specificity and affinity to the DBD-F.

Tryptophan fluorescence quenching has been used previously to determine changes in RPA conformation upon phosphorylation of the N-terminal domain of RPA32 (58–61). By assessing tryptophan quenching of RPA by FPA and subsequent fluorescence anisotropy competition assays, we demonstrate that FPA binds the DBD-F of RPA. Additionally, the comparison of tryptophan fluorescence quenching of full-length RPA, RPAΔF and the RPA (R41E, R43E) mutant in the presence of FPA provide evidence that FPA induces a structural rearrangement involving DBD-F and DBDs A–E. We currently do not know which of the eight tryptophan residues in DBDs A–E that are quenched upon FPA binding. However, ssDNA is capable of quenching four residues that reside in the DBDs A–D, W212, W361, W528 and W107(RPA32), respectively, (58) and our data shows that FPA does not affect ssDNA binding of RPA, making those residues less viable candidates for quenching by FPA-bound DBD-F. This suggests that W197, W414, W442 or W2 (RPA32) are quenched by FPA binding. FPA-induced conformational change is further supported by our data that revealed a difference in ligand binding to DBD-F^{MBP} compared with full length RPA. This was initially an unexpected result, as the flexibly linked DBD-F on RPA and the DBD-F^{MBP} should have the same affinity to ligand if DBD-F is a truly independent domain. Combined, our data imply an interaction between DBD-F and other RPA domains without preventing those same domains from binding to ssDNA (Figure 6A). We have previously shown FPA does not affect ssDNA binding to RPA (17), nor does p53TAD2 affect RPAΔF binding to ssDNA (Figure 3D), consistent with previous findings that full-length p53 did not inhibit RPA binding to ssDNA (62). These data, and the observed binding affinity differences of ligand to

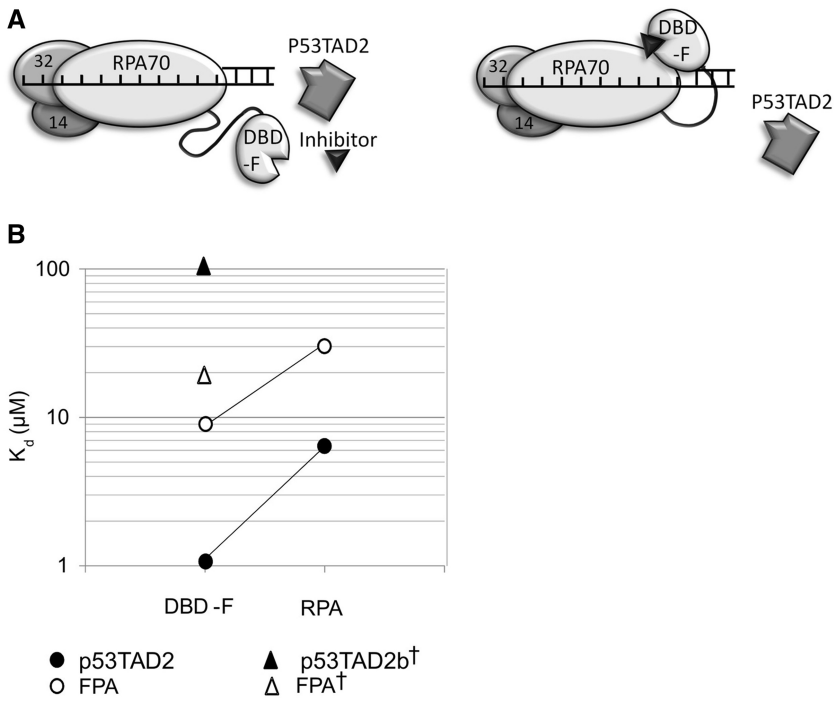

Figure 6. (**A**) Comparison of K_d values for p53 peptides and FPA binding to DBD-F and RPA. Solid and hollow circles are p53TAD2 and FPA K_d values, respectively, determined in this study. Solid and hollow triangles are p53TAD2b [15 aa peptide (aa 43–57 of p53)] and FPA K_d values, respectively, as reported in previous literature and therein denoted by (†)(63). (**B**) Depiction of competition between p53TAD2 and an inhibitor for the DBD-F accompanied by a change in conformation.

DBD-F^{MBP} and RPA, suggest that conformational changes occur in DBD-F in proximity to other RPA domains without affecting ssDNA binding of core domains DBD-A and DBD-B.

The RPA (R41E, R43E) mutation not only links the loss of RPA–p53 interaction to the loss of recombination in the *rfa-t11* yeast strain, but also raises the possibility that the helix destabilization activity of RPA may have relevance *in vivo*. RPA is commonly used in *in vitro* based recombination studies, initially binding ssDNA, and is eventually replaced by Rad51 before recombination with homologous dsDNA. Although RPA is thought to serve merely to deconvolute the ssDNA substrate before Rad51 binding, there could be a DBD-F–ssDNA intermediate step that is essential for efficient recombination to occur. The K45E mutation in *rfa-t11* has a deficit in catalysing recombination in these assays, which has been attributed to a loss of protein–protein binding (7). We suggest that both protein–protein and protein–DNA interactions with DBD-F may be important in the recombination process.

The crystal structure of the DBD-F, valuable as it has been for determining the spatial organization of the domain, offers only one conformation within a wide range of possible conformations. We previously used this crystal structure to model FPA and Rad9 binding to DBD-F (17); however, the molecular docking of FPA predicted an affinity that was much lower than the actual *in vitro* binding affinity. By determining an optimal binding conformation towards FPA, we demonstrate how the basic cleft of the DBD-F changes shape dramatically to confine the ligand. Multiple conformational changes are possible that are initiated by different ligands, as well as DBD-F contact with the remainder of RPA. Based on the relative binding parameters of the new conformation of RPA towards FPA, we are more confident in using this model to identify new inhibitors of DBD-F *in silico*.

Competition displacement studies of a similar p53 fragment and FPA have been reported (63). The reported binding constant reflected markedly weaker binding, 100 μM vs. 1 μM for p53TAD2 (Figure 6B). For FPA, the binding constant was also reported as weaker (18 μM vs. 9 μM). Although we can appreciate differences in apparent binding due to small changes in peptide sequence and assay conditions, we cannot account for the 50-fold difference in the ratios of binding constants (FPA:p53TAD2 peptide) between these two studies.

The involvement of RPA in several DNA modulatory activities hinges upon its ability to bind multiple disparate substrates. Many of these activities are dependent on the versatility of DBD-F, which offers a binding site for both protein and ssDNA, and harbours a site necessary for DNA unwinding. Further study with FPA and DBD-F may resolve more in-depth aspects of RPA in DNA metabolic activities.

SUPPLEMENTARY DATA

Supplementary Data are available at NAR Online: Supplementary Figures 1–4.

ACKNOWLEDGEMENTS

We thank Drs Marc Wold and James Wahl for kindly providing reagents and Adam Mosel for graphical assistance.

FUNDING

American Cancer Society [ACS RSG-10-031-01-CCG to G.G.O.]; Nebraska Department of Health and Human Services [2011–25 to G.G.O.]; National Institutes of Health (NIH) [P20RR018759 to G.G.O., P20-RR01875, GM59346, RR015468 to L.J.P.]. Funding for open access charge: NIH [P20RR018759]; American Cancer Society [RSG1003101CCG].

Conflict of interest statement. None declared.

REFERENCES

1. Oakley,G.G. and Patrick,S.M. (2010) Replication protein A: directing traffic at the intersection of replication and repair. *Front. Biosci.*, **15**, 883–900.
2. Wold,M.S. (1997) Replication protein A: a heterotrimeric, single-stranded DNA-binding protein required for eukaryotic DNA metabolism. *Annu. Rev. Biochem.*, **66**, 61–92.
3. Patrick,S.M. and Turchi,J.J. (1999) Replication protein A (RPA) binding to duplex cisplatin-damaged DNA is mediated through the generation of single-stranded DNA. *J. Biol. Chem.*, **274**, 14972–14978.
4. Lao,Y., Lee,C.G. and Wold,M.S. (1999) Replication protein A interactions with DNA. 2. Characterization of double-stranded DNA-binding/helix-destabilization activities and the role of the zinc-finger domain in DNA interactions. *Biochemistry*, **38**, 3974–3984.
5. Treuner,K., Ramsperger,U. and Knippers,R. (1996) Replication protein A induces the unwinding of long double-stranded DNA regions. *J. Mol. Biol*, **259**, 104–112.
6. Daughdrill,G.W., Ackerman,J., Isern,N.G., Botuyan,M.V., Arrowsmith,C., Wold,M.S. and Lowry,D.F. (2001) The weak interdomain coupling observed in the 70 kDa subunit of human replication protein A is unaffected by ssDNA binding. *Nucleic Acids Res.*, **29**, 3270–3276.
7. Kantake,N., Sugiyama,T., Kolodner,R.D. and Kowalczykowski,S.C. (2003) The recombination-deficient mutant RPA (rfa1-t11) is displaced slowly from single-stranded DNA by Rad51 protein. *J. Biol. Chem.*, **278**, 23410–23417.
8. Kim,H.S. and Brill,S.J. (2001) Rfc4 interacts with Rpa1 and is required for both DNA replication and DNA damage checkpoints in Saccharomyces cerevisiae. *Mol. Cell. Biol.*, **21**, 3725–3737.
9. Haring,S.J., Mason,A.C., Binz,S.K. and Wold,M.S. (2008) Cellular functions of human RPA1. Multiple roles of domains in replication, repair, and checkpoints. *J. Biol. Chem.*, **283**, 19095–19111.
10. Oakley,G.G., Tillison,K., Opiyo,S.A., Glanzer,J.G., Horn,J.M. and Patrick,S.M. (2009) Physical interaction between replication protein A (RPA) and MRN: involvement of RPA2 phosphorylation and the N-terminus of RPA1. *Biochemistry*, **48**, 7473–7481.
11. Li,R. and Botchan,M.R. (1993) The acidic transcriptional activation domains of VP16 and p53 bind the cellular replication protein A and stimulate in vitro BPV-1 DNA replication. *Cell*, **73**, 1207–1221.
12. He,Z., Brinton,B.T., Greenblatt,J., Hassell,J.A. and Ingles,C.J. (1993) The transactivator proteins VP16 and GAL4 bind replication factor A. *Cell*, **73**, 1223–1232.
13. Dutta,A., Ruppert,J.M., Aster,J.C. and Winchester,E. (1993) Inhibition of DNA replication factor RPA by p53. *Nature*, **365**, 79–82.

14. Olson,E., Nievera,C.J., Liu,E., Lee,A.Y., Chen,L. and Wu,X. (2007) The Mre11 complex mediates the S-phase checkpoint through an interaction with replication protein A. *Mol. Cell. Biol.*, **27**, 6053–6067.
15. Xu,X., Vaithiyalingam,S., Glick,G.G., Mordes,D.A., Chazin,W.J. and Cortez,D. (2008) The basic cleft of RPA70N binds multiple checkpoint proteins, including RAD9, to regulate ATR signaling. *Mol. Cell. Biol.*, **28**, 7345–7353.
16. Ball,H.L., Ehrhardt,M.R., Mordes,D.A., Glick,G.G., Chazin,W.J. and Cortez,D. (2007) Function of a conserved checkpoint recruitment domain in ATRIP proteins. *Mol. Cell. Biol.*, **27**, 3367–3377.
17. Glanzer,J.G., Liu,S. and Oakley,G.G. (2011) Small molecule inhibitor of the RPA70 N-terminal protein interaction domain discovered using in silico and in vitro methods. *Bioorg. Med. Chem.*, **19**, 2589–2595.
18. Vogelstein,B., Lane,D. and Levine,A.J. (2000) Surfing the p53 network. *Nature*, **408**, 307–310.
19. Levine,A.J. (1997) p53, the cellular gatekeeper for growth and division. *Cell*, **88**, 323–331.
20. Joerger,A.C. and Fersht,A.R. (2010) The tumor suppressor p53: from structures to drug discovery. *Cold Spring Harb. Perspect. Biol.*, **2**, a000919.
21. Candau,R., Scolnick,D.M., Darpino,P., Ying,C.Y., Halazonetis,T.D. and Berger,S.L. (1997) Two tandem and independent sub-activation domains in the amino terminus of p53 require the adaptor complex for activity. *Oncogene*, **15**, 807–816.
22. Vise,P.D., Baral,B., Latos,A.J. and Daughdrill,G.W. (2005) NMR chemical shift and relaxation measurements provide evidence for the coupled folding and binding of the p53 transactivation domain. *Nucleic Acids Res.*, **33**, 2061–2077.
23. Rajagopalan,S., Andreeva,A., Teufel,D.P., Freund,S.M. and Fersht,A.R. (2009) Interaction between the transactivation domain of p53 and PC4 exemplifies acidic activation domains as single-stranded DNA mimics. *J. Biol. Chem.*, **284**, 21728–21737.
24. Bochkareva,E., Kaustov,L., Ayed,A., Yi,G.S., Lu,Y., Pineda-Lucena,A., Liao,J.C., Okorokov,A.L., Milner,J., Arrowsmith,C.H. *et al.* (2005) Single-stranded DNA mimicry in the p53 transactivation domain interaction with replication protein A. *Proc. Natl Acad. Sci. USA*, **102**, 15412–15417.
25. Rajagopalan,S., Andreeva,A., Rutherford,T.J. and Fersht,A.R. (2010) Mapping the physical and functional interactions between the tumor suppressors p53 and BRCA2. *Proc. Natl Acad. Sci. USA*, **107**, 8587–8592.
26. Kaustov,L., Yi,G.S., Ayed,A., Bochkareva,E., Bochkarev,A. and Arrowsmith,C.H. (2006) p53 transcriptional activation domain: a molecular chameleon? *Cell Cycle*, **5**, 489–494.
27. Sirbu,B.M., Lachmayer,S.J., Wulfing,V., Marten,L.M., Clarkson,K.E., Lee,L.W., Gheorghiu,L., Zou,L., Powell,S.N., Dahm-Daphi,J. *et al.* (2011) ATR-p53 restricts homologous recombination in response to replicative stress but does not limit DNA interstrand crosslink repair in lung cancer cells. *PLoS One*, **6**, e23053.
28. Pretto,D.I., Tsutakawa,S., Brosey,C.A., Castillo,A., Chagot,M.E., Smith,J.A., Tainer,J.A. and Chazin,W.J. (2010) Structural dynamics and single-stranded DNA binding activity of the three N-terminal domains of the large subunit of replication protein A from small angle X-ray scattering. *Biochemistry*, **49**, 2880–2889.
29. Henricksen,L.A., Umbricht,C.B. and Wold,M.S. (1994) Recombinant replication protein A: expression, complex formation, and functional characterization *J. Biol. Chem.*, **269**, 11121–11132.
30. Sheffield,P., Garrard,S. and Derewenda,Z. (1999) Overcoming expression and purification problems of RhoGDI using a family of "parallel" expression vectors. *Protein Expr. Purif.*, **15**, 34–39.
31. Huibregtse,J.M., Scheffner,M. and Howley,P.M. (1991) A cellular protein mediates association of p53 with the E6 oncoprotein of human papillomavirus types 16 or 18. *EMBO J.*, **10**, 4129–4135.
32. Press,W.H., Teukolsky,S.A., Vetterling,W.T. and Flannery,B.P. (2007) *Numerical Recipes: The Art of Scientific Computing*, 3rd edn. Cambridge University Press, Cambridge England.
33. Draper,N.R. and Smith,H. (1981) *Applied Regression Analysis*, 2nd edn. John Wiley and Sons.
34. Van Der Spoel,D., Lindahl,E., Hess,B., Groenhof,G., Mark,A.E. and Berendsen,H.J. (2005) GROMACS: fast, flexible, and free. *J. Comput. Chem.*, **26**, 1701–1718.
35. Lee,M.R., Duan,Y. and Kollman,P.A. (2001) State of the art in studying protein folding and protein structure prediction using molecular dynamics methods. *J. Mol. Graph. Model.*, **19**, 146–149.
36. Jorgensen,W.L., Chandrasekhar,J., Buckner,J.K. and Madura,J.D. (1986) Computer simulations of organic reactions in solution. *Ann. N. Y. Acad. Sci.*, **482**, 198–209.
37. Villa,A., Mark,A.E., Saracino,G.A., Cosentino,D.P., Moro,G. and Salmona,M. (2006) Conformational polymorphism of the PrP106-126 peptide in different environments: a molecular dynamics study. *J. Phys. Chem. B*, **110**, 1423–1428.
38. Bussi,G., Donadio,D. and Parrinello,M. (2007) Canonical sampling through velocity rescaling. *J. Chem. Phys.*, **126**, 014101.
39. Hess,B., Bekker,H., Berendsen,H.J.C. and Fraaije,J.G.E.M. (1997) LINCS: a linear constraint solver for molecular simulations. *J Comput. Chem.*, **18**, 1463–1472.
40. Miyamoto,S. and Kollman,P.A. (1992) Settle—an analytical version of the shake and rattle algorithm for rigid water models. *J. Comput. Chem.*, **13**, 952–962.
41. Tironi,I., Sperb,R., Smith,P. and van Gunsteren,W. (1995) A generalized reaction field method for molecular-dynamics simulations. *J. Phys. Chem.*, **102**, 5451–5459.
42. van der Spoel,D., Lindahl,E., Hess,B., van Buuren,A.R., Apol,E., Meulenhoff,P.J., Tieleman,D.P., Sijbers,A.L., Teemu,M. and Feenstra,K.A. (2010), *Gromacs user manual version 4.5.4*.
43. Atilgan,A.R., Durell,S.R., Jernigan,R.L., Demirel,M.C., Keskin,O. and Bahar,I. (2001) Anisotropy of fluctuation dynamics of proteins with an elastic network model. *Biophys. J.*, **80**, 505–515.
44. Bakan,A., Meireles,L.M. and Bahar,I. (2011) ProDy: protein dynamics inferred from theory and experiments. *Bioinformatics*, **27**, 1575–1577.
45. Trott,O. and Olson,A.J. (2010) AutoDock Vina: improving the speed and accuracy of docking with a new scoring function, efficient optimization, and multithreading. *J. Comput. Chem.*, **31**, 455–461.
46. Wolf,L.K. (2009) Digital Briefs. *Chemical & Engineering News*, **87**, 31.
47. Seeliger,D. and de Groot,B.L. (2010) Ligand docking and binding site analysis with PyMOL and Autodock/Vina. *J. Comput. Aided Mol. Des.*, **24**, 417–422.
48. Wiyono,B., Tachibana,S. and Tinambunan,D. (2007) Reaction of abietic acid with maleic anhydride and fumaric acid and attempts to find the fundamental component of fortified rosin. *Pak. J. Biol. Sci.*, **10**, 1588–1595.
49. Umezu,K., Sugawara,N., Chen,C., Haber,J.E. and Kolodner,R.D. (1998) Genetic analysis of yeast RPA1 reveals its multiple functions in DNA metabolism. *Genetics*, **148**, 989–1005.
50. Zou,L. and Elledge,S.J. (2003) Sensing DNA damage through ATRIP recognition of RPA-ssDNA complexes. *Science*, **300**, 1542–1548.
51. Jacobs,D.M., Lipton,A.S., Isern,N.G., Daughdrill,G.W., Lowry,D.F., Gomes,X. and Wold,M.S. (1999) Human replication protein A: global fold of the N-terminal RPA-70 domain reveals a basic cleft and flexible C-terminal linker. *J. Biomol. NMR*, **14**, 321–331.
52. Nussinov,R. and Ma,B. (2012) Protein dynamics and conformational selection in bidirectional signal transduction. *BMC Biol.*, **10**, 2.
53. Boehr,D.D. (2012) Promiscuity in protein-RNA interactions: conformational ensembles facilitate molecular recognition in the spliceosome: conformational diversity in U2AF(6)(5) facilitates binding to diverse RNA sequences. *Bioessays*, **34**, 174–180.
54. Fanning,E., Klimovich,V. and Nager,A.R. (2006) A dynamic model for replication protein A (RPA) function in DNA processing pathways. *Nucleic Acids Res.*, **34**, 4126–4137.
55. Romanova,L.Y., Willers,H., Blagosklonny,M.V. and Powell,S.N. (2004) The interaction of p53 with replication protein A mediates suppression of homologous recombination. *Oncogene*, **23**, 9025–9033.
56. Shammas,M.A., Shmookler Reis,R.J., Koley,H., Batchu,R.B., Li,C. and Munshi,N.C. (2009) Dysfunctional homologous

recombination mediates genomic instability and progression in myeloma. *Blood*, **113**, 2290–2297.
57. Plo,I., Nakatake,M., Malivert,L., de Villartay,J.P., Giraudier,S., Villeval,J.L., Wiesmuller,L. and Vainchenker,W. (2008) JAK2 stimulates homologous recombination and genetic instability: potential implication in the heterogeneity of myeloproliferative disorders. *Blood*, **112**, 1402–1412.
58. Liu,Y., Kvaratskhelia,M., Hess,S., Qu,Y. and Zou,Y. (2005) Modulation of replication protein A function by its hyperphosphorylation-induced conformational change involving DNA binding domain B. *J. Biol. Chem.*, **280**, 32775–32783.
59. Patrick,S.M. and Turchi,J.J. (2001) Stopped-flow kinetic analysis of replication protein A-binding DNA: damage recognition and affinity for single-stranded DNA reveal differential contributions of k(on) and k(off) rate constants. *J. Biol. Chem.*, **276**, 22630–22637.
60. Roy,R., Kozlov,A.G., Lohman,T.M. and Ha,T. (2009) SSB protein diffusion on single-stranded DNA stimulates RecA filament formation. *Nature*, **461**, 1092–1097.
61. Kim,C., Paulus,B.F. and Wold,M.S. (1994) Interactions of human replication protein A with oligonucleotides. *Biochemistry*, **33**, 14197–14206.
62. Miller,S.D., Moses,K., Jayaraman,L. and Prives,C. (1997) Complex formation between p53 and replication protein A inhibits the sequence-specific DNA binding of p53 and is regulated by single-stranded DNA. *Mol.Cell. Biol.*, **17**, 2194–2201.
63. Souza-Fagundes,E.M., Frank,A.O., Feldkamp,M.D., Dorset,D.C., Chazin,W.J., Rossanese,O.W., Olejniczak,E.T. and Fesik,S.W. (2012) A high-throughput fluorescence polarization anisotropy assay for the 70N domain of replication protein A. *Anal. Biochem.*, **421**, 742–749.